Co-variability of Bars in a Multi-bar Nearshore Zone Determined with Canonical Correlation Analysis (CCA)

Grzegorz Różyński

Institute of Hydro-Engineering of the Polish Academy of Sciences,
ul. Kościerska 7, 80-953 Gdańsk, Poland

Abstract

Nearshore bed variations of the southern Baltic shore were investigated with the aim of detecting co-variability among bed forms of a multi-bar system. The studied area is located at IBW PAN Coastal Research Station at Lubiatowo. The beach consists of fine sand of median grain equal to 0.22 mm, is mildly sloping and boasts multiple (usually 4) bars, which is typical for the coast in the southern Baltic. Data on bed topography were collected along 27 lines, equally spanned every 100 m, since 1987 to 1999, usually twice a year. Fairly high alongshore bed homogeneity made it possible to choose one representative profile for which the CCA method was employed. The method demonstrated considerable potential for detecting co-variability of bed features in the nearshore zone. The results show that some 80% of variability in the region of the offshore slope of the outermost bar can be attributed to variations of Dean equilibrium profiles. The portion of variability of the two innermost bars due to variations of equilibrium profiles equals 40%. Horizontal counter-movements of outer and inner bars can be responsible for some 20%. The remaining 40% should be related to highly variable short time scale phenomena like breakers and wave driven currents in the vicinity of inner bars.

1. Introduction

Morphodynamic processes in the nearshore zone are complex, highly nonlinear phenomena involving morphological features in a wide range of spatial and temporal scales (De Vriend 1991, Larson and Kraus 1995). Even though the insight into the physical mechanisms of these processes is growing continuously, it is still insufficient to properly understand, depict and predict the behavior of many coastal systems. However, the number of high quality data sets on coastal morphology is growing simultaneously, thus providing the possibility of deriving valuable information on morphological properties by means of computer-intensive analysis and data-driven modelling (Larson et al. 2000b, Southgate et al. 2000). Such

methods were originally applied to meteorological and oceanographic data, and only recently has their use been extended to studies on coastal morphology.

In analysis of large data sets it is a common practice to split state vectors (i.e. the morphological data) into signal and noise. The signal is usually featured by a few patterns representing behaviour of the process in question, whose physical interpretation we seek. The noise is believed to contain all secondary processes the joint influence on the studied process of which is deemed negligible. A signal can be specified in various ways extending from subjectively defined patterns, e.g. a definition of a longshore bar, to patterns constructed to optimize some statistical measure. Classic examples are empirical orthogonal functions (EOF), (Winant et al. 1975), Aubrey 1979, Wijnberg and Terwindt 1995, Larson et al. 1999), where the signal is determined by dominant eigenmodes of a covariance matrix in the spatial domain (the EOF modes). Their physical interpretation is usually a crucial point of a study. Apart from that the EOF method offers a powerful filtration potential, i.e. we can construct the signal by retaining as many EOF modes as necessary to achieve a prescribed threshold of the overall raw state vector variance, e.g. 95%. The signal can also be extracted from a covariance matrix in the temporal domain, for which we determine eigenelements. This technique is known as singular spectrum analysis (SSA), where we investigate one variable, or multi-channel SSA (MSSA), where we study a vector time series (Vautard et al. 1992). From the most significant eigenelements we can derive several key patterns accounting for most variability over time. They usually represent trends, oscillations, deterministic chaos etc., for which we again search physical interpretation. In coastal morphology SSA was used by Southgate et al. (2000) to evaluate long-term trends of shoreline position variations at several beaches around the world. Różyński et al. (2000) employed SSA to determine forced and self organized shoreline response for a beach in the southern Baltic Sea at IBW PAN Coastal Research Station (CRS) at Lubiatowo.

Principal oscillation patterns (POP) is a slightly different technique. It was developed to predict future states of large systems (Hasselmann 1988), so this technique offers an opportunity for constructing data-driven models that base on fully incorporated large data sets. The POP system matrix relates current and previous states of a system, and the character of its eigenelements determines their relevance for prediction purposes. Różyński and Jansen (2000) applied POP with EOF signal pre-filtering to come up with the data-driven model of bed evolution in the nearshore zone at Lubiatowo.

Canonical correlation analysis (CCA) allows for investigation of relationships between two simultaneously observed vector time series. In other words, we try to reconstruct one field (predictand) with the other field (predictor). Discrepancies between predicted and recorded values of a predictand determine the relevance of this method in a particular application. Widely used in climate studies, it has not been frequently applied in coastal engineering. Larson et al. (2000a) employed

CCA to study the relationship between beach profiles and waves at Duck, USA. In the current study, the CCA was utilized to assess the influence of bed forms on each other in the multi-bar environment of the beach at CRS Lubiatowo. First, the Lubiatowo beach is described together with the morphological data sets collected there. Then a brief description of the CCA method, together with EOF signal pre-filtering is given. Finally, the CCA is employed in records of bed topography along a representative beach profile, collected between 1987 and 1999. The records were divided in various ways to analyze different predictor/predictand pairs. Moreover, bed equilibrium profiles were computed and used as predictors.
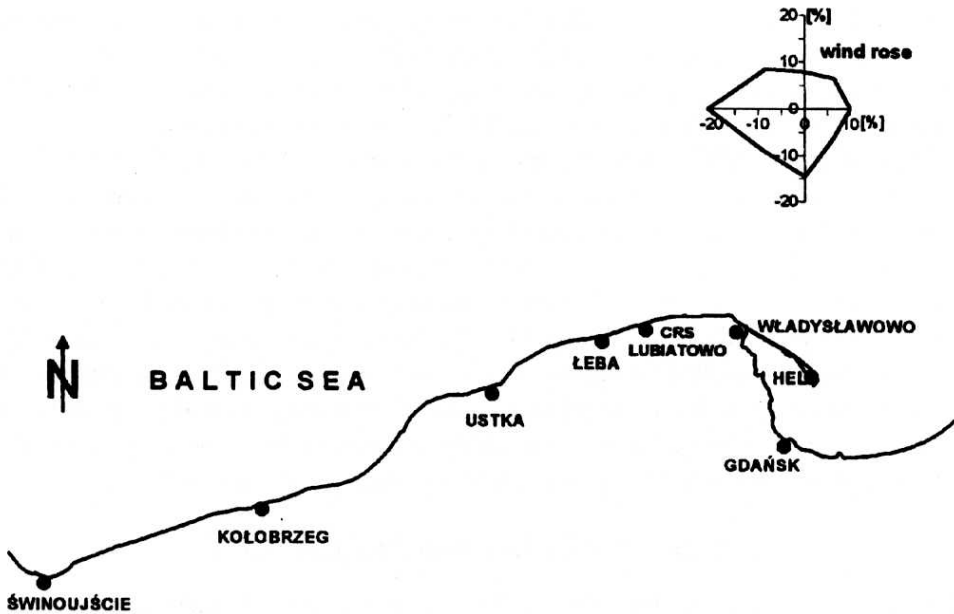
Fig. 1. Location of CRS Lubiatowo on Polish coast

2. Field Site and Data

The CRS Lubiatowo is situated on the Polish Coast, facing the southern part of the Baltic Sea (Fig. 1). The beach there has a mild slope $\tan \alpha = 1$–1.5%, is build of fine sand of median grain size $D_{50} = 0.22$ mm and usually encompasses multiple longshore bars. They contribute to multiple breakers frequently observed in the surf zone. The oblique long-term energy flux triggers predominantly west to east littoral drift. Records taken over years indicate that during average storms the significant wave height outside the surf zone (depth h about 20 m) usually

reaches H_s = 2–2.5 m with a mean period T = 5–7 s. As the waves propagate onshore their energy is dissipated and when h = 2–3 m, the average wave height typically equals $\overline{H}$ = 0.5–1 m with $\overline{T}$ = 4–5 s, Pruszak et al. (1999). For h = 1 m it reduces during storms to 0.3–0.5 m. The influence of tides is negligible due to the isolation of the Baltic Sea from the Atlantic Ocean by the Danish Straits.

Long-term bathymetric surveys have proved that the beach at Lubiatowo normally exhibits a system of four stable bars, cf. Różyński et al. (1999). The innermost bar is located some 120–170 m from a local baseline with depth over crest equal to 1–1.5 m. The 2nd bar is situated 200–300 m from the baseline and its crest lies 2–2.5 m below the mean sea level. Two outer bars are 400–500 m and 600–800 m away from the base and their depths at crest are 3.5–4 m and 5–5.5 m. An ephemeral 5th bar occasionally develops in very close proximity of the shoreline and it may come ashore as a small beach berm. The bars do not migrate but only oscillate about their average locations (Pruszak et al. 1997 and 1999). The baseline is fixed on a dune crest some 10–50 m from the shoreline.

Measurements of bed topography were initiated in 1964 and since 1987 they have been executed upon a fairly regular basis, usually twice a year along 27 cross-shore lines, uniformly spanned every 100 m, every 10 m between consecutive points on one line. Enumeration of those lines originates from the history of the local geodetic base at CRS Lubiatowo; initially baseline points 3, 4... 10, east of point 3 were fixed, then the points 11, 12... 29 were added west of point 3. The lines are usually sampled in spring and autumn after and before winter storms. Naturally, such an order is sometimes violated and over several years only one record was taken. Furthermore, some spring records could occur early in summer and some other autumn surveys were actually done in the late summer.

3. Canonical Correlation Analysis (CCA)

CCA was developed by Hotelling (1935) as a method characterizing linkages between sets of test scores. The potential value of this technique in geophysical studies was first pointed out by Glahn (1968) and then by Davis (1976, 1978). The version presented in this paper includes pre-filtering of raw data sets with EOF and stems from Graham (1990), who utilized results of previous studies (Graham 1987a, b), Barnett & Preisendorfer 1987).

In the traditional approach the problem can be formulated as follows:
Let us begin with two data sets in the form of vector time series $Y_{t,y}$ and $Z_{t,z}$, where t indicates observations in time of spatial variations y and z:

$$t = 1, 2, \ldots nt, \quad y = 1, 2, \ldots ny, \quad z = 1, 2, \ldots nz.$$

The number of observations nt **must** be the same for each data set and the numbers of spatial points need not be equal. After removal of mean values of each spatial location y and z, we construct linear combinations of Y and Z respectively,

so that new variables $U_{m,t}$ and $V_{m,t}$ are maximally correlated, U_1 is related to V_1, U_2 to V_2 and so forth. In addition it is required that each U and V has a unit variance and the U's and V's are orthogonal. Hence, we arrive at the following characteristics:

$$\frac{\langle U_m V_n \rangle}{(\langle U_m^2 \rangle \langle V_n^2 \rangle)^{1/2}} = \max \quad m = n, \tag{1}$$

$$\langle U_m V_n \rangle = 0 \quad m \neq n, \tag{2}$$

$$\langle U_m U_n = 1 \rangle \quad m = n, \tag{3}$$

$$\langle U_m U_n \rangle = 0 \quad m \neq n, \tag{4}$$

$$\langle V_m V_n \rangle = 1 \quad m = n, \tag{5}$$

$$\langle V_m V_n \rangle = 0 \quad m \neq n. \tag{6}$$

Angle brackets $< \ldots >$ denote expected value of the vector product over a period of time, e.g.:

$$\langle U_m U_n \rangle = \frac{1}{nt} \sum_{t=1}^{n} t U_{m,t} U_{n,t}.$$

Given constraints (1), (3) and (5) the desired weights for transforming Y into U and Z into V can be found after solution of the eigenvalue problem:

$$\left[(Y^t Y)^{-1} (Y^t Z) (Z^t Z)^{-1} (Z^t Y) - \mu I \right] = 0 \tag{7}$$

where the letter t here indicates the matrix transpose. The eigenvalues μ_m (often denoted μ_m^2) are squared **canonical correlations** sought in Eq. (1). The concomitant **eigenvectors** $R_{y,m}$ provide the required weights for transforming Y into U. In matrix notation:

$$U = YR. \tag{8}$$

By **canonical mode** m we will understand the canonical correlation μ_m with the associated eigenvector $R_{y,m}$. The maximum number of canonical modes is determined by the rank of the quadruple product in Eq. (7); for large natural systems it will almost certainly be equal to the number of observations nt. When we swap Y for Z in Eq. (7) we obtain the same canonical correlations μ_m and the eigenvectors Q for transforming Z into V, i.e. $V = ZQ$. Let us now denote the Y field as **predictor** and Z as **predictand**. Predictor is linked to the predictand with the matrix of regression coefficients S relating the values of predictor canonical mode temporal amplitudes U to the individual points in the predictand field Z. Due to orthogonality and unit variance of U, this matrix can be evaluated from:

$$S_{m,z} = \langle U_m Z_z \rangle , \tag{9}$$

where m is the canonical mode index and z the spatial index of elements of Z. In matrix notation the regression equation takes the form:

$$\hat{Z} = U'S, \tag{10}$$

where $\hat{Z}$ are predictions of Z with the Y field. Using Eq. (8), we can write this equation in "real" space:

$$\hat{Z} = YRS. \tag{11}$$

The CCA procedure outlined above can be enriched with EOF signal pre-filtering and compression. Since most variance in Y and Z is contained in a few EOF modes and the number of spatial points (ny and nz) is usually large, the EOF expansion guarantees matrix conversion in Eq. (7), whose rank usually equals the number of realizations nt, being less than ny or nz. The resultant matrices have substantially smaller dimensions leading to reduction of memory requirements and computation time. Furthermore, the expansion allows for thorough inspection of either of the fields by investigating the behaviour of dominant EOF modes. The modes reflecting residual variability can be treated as noise and safely skipped.

The EOF expansion consists in calculation of covariance matrices of both data sets and obtaining their eigenstructures. For the Y field for example, the covariance matrix is calculated as:

$$\Gamma = \frac{1}{nt}Y'Y, \tag{12}$$

which means that the individual elements of Γ are given by:

$$\Gamma_{i,j} = \langle Y_{y_i} Y_{y_j} \rangle \; i, j = 1, 2, \ldots ny. \tag{13}$$

The eigenstructure of this matrix consists of eigenvalues κ equal to the variance of a given mode and the concomitant spatial eigenvectors e, usually scaled to unit length. The associated temporal amplitudes (EOF coefficients or principal components) are obtained by:

$$\alpha = Ye. \tag{14}$$

Their variance is equal to the corresponding eigenvalue, i.e. $\langle \alpha_i^2 \rangle = \kappa_i$.

Repeating the above procedure with the Z field, we obtain the eigenvalues λ, eigenvectors f and amplitudes β. Hence, both fields can be expressed in terms of EOF modes:

$$Y = \alpha e', \tag{15}$$

$$Z = \beta f'. \tag{16}$$

The number of EOF modes retained for CCA analysis was denoted $n\alpha$ and $n\beta$ for Y and Z fields respectively. Cross-correlation of both fields can be expressed by temporal amplitudes α and β:

$$C = \Gamma_\kappa^{-1}\alpha'\beta\Gamma_\lambda^{-1}. \tag{17}$$

Γ_κ and Γ_λ represent diagonal matrices of inverse square roots of the eigenvalues of EOF decomposition of Y and Z respectively, e.g.:

$$\Gamma^{-1}_{\kappa(i,i)} = \frac{1}{\kappa_i^{1/2}}. \tag{18}$$

The analogue of the quadruple matrix product in Eq. (7) can now be obtained as:

$$C* = CC^t \tag{19}$$

with the eigenvalue problem:

$$(C* - \mu I) = 0. \tag{20}$$

The eigenvalues μ yield squared correlations between the temporal amplitudes of the canonical modes, while the associated unit length vectors R provide weights for combining the EOF modes to come up with the canonical amplitudes:

$$U = \alpha \Gamma^{-1}_\kappa R. \tag{21}$$

The matrix Γ^{-1}_κ normalizes the EOF amplitudes to unit variance, so the U's variance equals unity as well.

The percentage of total variance in the Y field accounted for by each canonical mode can be calculated, because the eigenvector elements $R_{i,m}$ are correlations between the temporal amplitudes of EOF mode i mode (α_i) and canonical mode m (U_m). Hence, if the percentage of total variance in the Y field, accounted for by each EOF mode equals P_i, then that of total variance in this field accounted for by canonical mode m is given by:

$$P^y_m = \sum_{i=1}^{n\alpha} R^2_{i,m} P_i. \tag{22}$$

If the number of canonical modes is equal to nm, the sum of P^y_k gives the percentage of total variance of the predictor field accounted for by predictor canonical variables.

Apart from canonical temporal amplitudes U, which are linear combinations of the temporal amplitudes of the EOF-s we can also define canonical spatial patterns g as linear combinations of the spatial EOF patterns:

$$g = e\Gamma^{-1}_\kappa R. \tag{23}$$

Here the matrix Γ^{-1}_κ scales the spatial EOF patterns e so that the projections U of the predictor data Y onto the patterns g,

$$Yg = U \tag{24}$$

retain the unit variance, as required by Eq. (3).

The predictand side of the canonical modes can be calculated as a solution of the eigenvalue problem:

$$(C^{**} - \mu I) = 0,\tag{25}$$

where $C^{**} = C^t C$. As a result we obtain the same eigenvalues as in Eq. (20) plus the eigenvectors Q combining the predictand EOF-s. Temporal and spatial patterns of the predictand side are then calculated analogously to Eqs. (21) and (23):

$$V = \beta \Gamma_\lambda^{-1} Q,\tag{26}$$

$$h = f \Gamma_\lambda^{-1} Q.\tag{27}$$

Continuing the analogy we can calculate the fraction of the total variance of the Z field for the canonical mode m:

$$P_m^z = \sum_{j=1}^{n\beta} Q_{j,m}^2 L_j,\tag{28}$$

where L_j denotes the percentage of total variance in the Z field held by j predictand EOF. The sum of P_m^z quantifies the fraction of total variance in the Z field captured by predictand canonical variables.

The fraction of the predictand field variance retrievable by canonical predictors is given by:

$$P^* = \sum_{m=1}^{nm} P_z^m \mu_m.\tag{29}$$

This number provides a useful measure of co-variability between predictor and predictand fields. However, a more exact figure of merit, defining how much of the available predictand variance can be accounted for by the canonical regression model, is produced by:

$$P^\otimes = \frac{P^*}{\sum\limits_{j=1}^{n\beta} L_j},\tag{30}$$

i.e. P^* is divided by percentage of variance of input predictand EOF-s. Practically, these quantities are almost equivalent when the threshold of variance of input EOF-s in either field is high enough, say 95%. This can be achieved by suitable choice of $n\alpha$ and $n\beta$, so that $n\alpha = n\beta = \max(n\alpha_{95\%}, n\beta_{95\%}) = nm$.

The crucial issue of CCA analysis is the derivation of regression matrix, relating predictor field to the predictand. By virtue of orthonormality of predictor canonical variables U, we can relate them to input predictand EOF-s β, by taking the expectations:

$$S_{m,j} = \langle U_m \beta_j \rangle\tag{31}$$

so that we come up with the estimates:

$$\hat{\beta} = US. \tag{32}$$

Post-multiplying by f^t and using the identity $\hat{Z} = \hat{\beta} f^t$ we can calculate the estimates of the predictand field by predictor canonical variables:

$$\hat{Z} = USf^t. \tag{33}$$

Now, using Eq. (24), we can express these quantities with the original predictor field:

$$\hat{Z} = Yg\,Sf^t. \tag{34}$$

4. CCA Analysis of Multi-bar Shore at CRS Lubiatowo

22 measurements of the representative profile 4 from 100 to 900 m from the base were used in the study. Their dates are presented in Table 1. The choice of representative profile is partly explained in Fig. 2, where all records for profiles 4, 5, 6 and 7 are shown. They indicate that their behaviour is very similar. More remote profiles follow the same pattern, so the beach is uniform in the along-shore direction to a high extent, thus justifying the simplified approach with one representative profile. Moreover, not all measurements at other lines cover the desired distance 100–900 m.

Table 1. Dates of records of bed topography at CRS Lubiatowo

Spring	Autumn
16th May 1987	22nd Sep. 1987
28th Apr. 1988	5th Oct. 1988
24th May 1989	13th Sep. 1989
5th Jun. 1990	14th Aug. 1990
	29th Oct. 1991
21st May 1992	21st Oct. 1992
20th Jul. 1993	30th Sep. 1993
24th Apr. 1994	
	5th Oct. 1995
24th Aug. 1996	6th Oct. 1996
	5th Nov. 1997
26th Jun. 1998	23rd Nov. 1998
4th Jul. 1999	8th Sep. 1999

Before the CCA analysis was started both mean empirical profile and line of standard deviations of measurements were plotted as solid lines in Fig. 3. We can
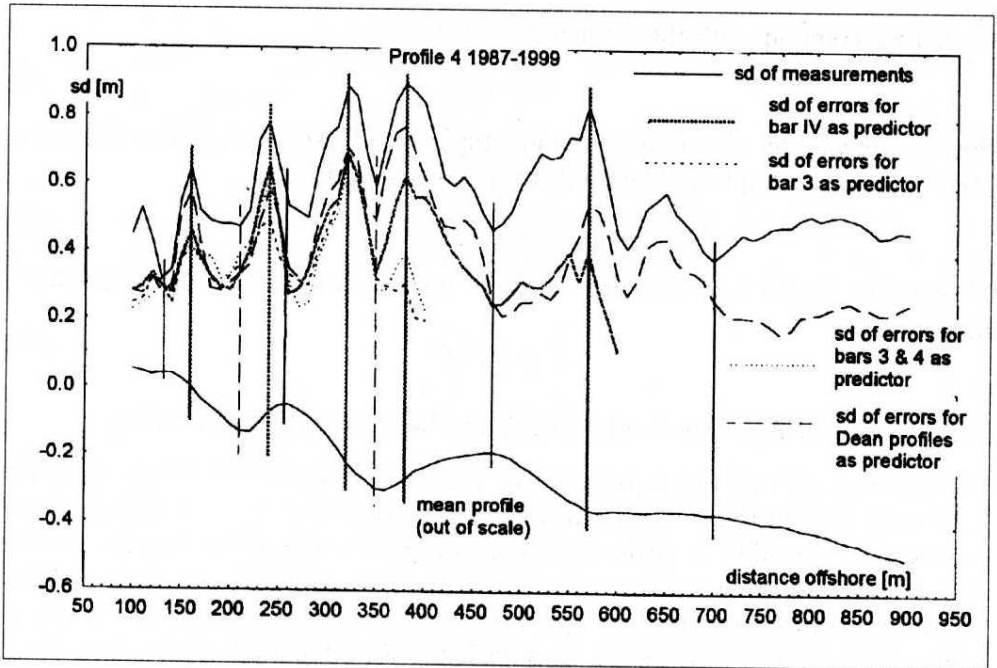
Fig. 2. Bed topography 1987–1999 for lines 4, 5, 6 and 7

see that standard deviations have minima over bar crests and troughs (the latter excepting the trough between bars 3 and 4). Maxima are associated with onshore and offshore slopes of bars. Such a pattern indicates that crests and troughs are fairly firmly fixed, while the slopes may approach both crests and troughs during oscillatory movements of bars, producing greater scatter of measurements. Hence, bar oscillations occur in fairly narrow bounds being limited by much more stable positions of crests and troughs.

A key point of every CCA study is the choice of predictor and predictand. In case of beach profiles the direction of incoming waves indicates to take one or more outer bars as predictors and treat inner bars as predictands. In such reasoning it is assumed that outer bars may control the behaviour of inner bars by the feedback between incoming waves and outer bars, i.e. the waves transform outer bars and are simultaneously transformed by rapid bed shoaling over them. This leads to the loss of wave energy due to breakers, thus inner bars are then exposed to reduced energy influx.

The first analysis was carried out for bar 4 as predictor (610–900 m) and bars 1, 2 and 3 as predictand (100–600 m), in order to assess the dependence of inner bars on the outermost bar. $nm = 9$ canonical modes correspond to 99.56% of total variance of the predictor and 95.86% of the predictand with $P^{\otimes} = 0.624$. For this regression predictions $\hat{Z}$ were computed together with discrepancies between
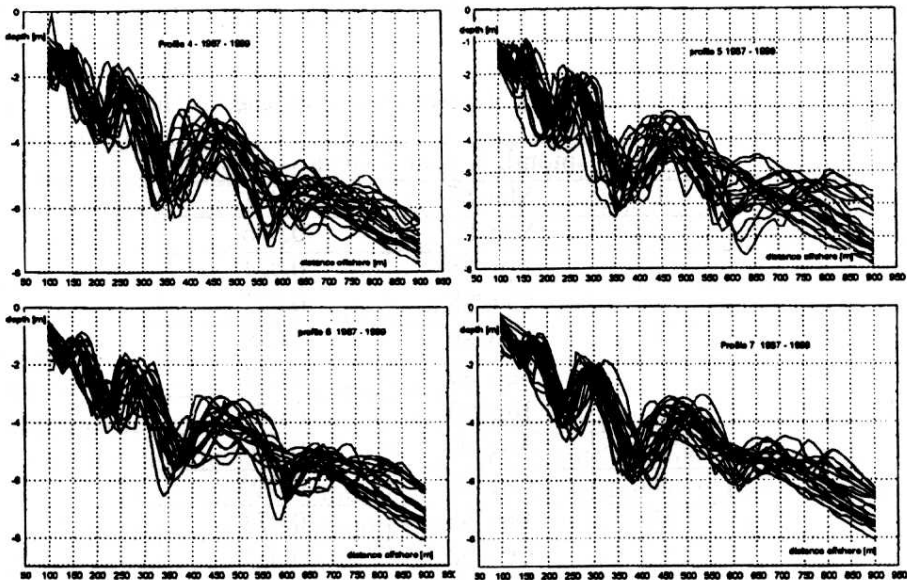
Fig. 3. Results of CCA analysis for different pairs of predictor and predictand

actual records and predictions $Z_d = Z - \hat{Z}$. The resultant standard deviations of prediction errors are plotted in Fig. 3 as a dense dotted line. This line shows that roughly speaking prediction errors are proportional to standard deviations of measurements, so positions of crests and trough are predicted with better accuracy than onshore and offshore slopes of bars. Average prediction error, computed as a mean value of all elements of Z_d matrix is equal to $w = 0.4$ m.

The 2nd analysis took positions of bars 1 and 2 as predictand (100–400 m) and bar 3 as predictor (410–620 m). 8 canonical modes correspond to 99.43% of the total variance of the predictor and 96% of the predictand. It is interesting, that $P^{\otimes} = 0.667$ $w = 0.37$ m, are very close to the previous results. The resemblance is even more striking when we analyze the line of standard deviations of prediction errors (dashed line in Fig. 3), which almost exactly matches its counterpart from the previous analysis.

The results hardly change when we use outer bars 3 and 4 as predictand (410–900 m), as with 8 canonical modes we obtain 97.36% of total predictor variability against 96% of the predictand's. Consequently, $P^{\otimes} = 0.647$, $w = 0.39$ m and the line of standard deviation of prediction errors, drawn in Fig. 3 as a fine dotted line, very consistently matches the results of the past two analyses. It can therefore be concluded that predictands and predictors must share a common feature, so that practically the same results are obtained for various combinations of predictor and

predictand. They also point out the upper threshold (roughly 60%) of variability of inner bars that can be explained by the variability of outer bars.

Table 2. Dean coefficients of recorded beach topography at line 4

No. Rec.	month & year	Dean coefficient
1	May'87	0.081
2	Sep.'87	0.076
3	Apr.'88	0.074
4	Oct.'88	0.072
5	May'89	0.078
6	Sep.'89	0.074
7	Jun.'90	0.073
8	Aug.'90	0.076
9	Oct.'91	0.080
10	May'92	0.077
11	Oct.'92	0.082
12	Jul.'93	0.073
13	Sep.'93	0.072
14	Apr.'94	0.078
15	Oct.'95	0.070
16	Aug.'96	0.073
17	Oct.'96	0.070
18	Nov.'97	0.072
19	Jun.'98	0.071
20	Nov.'98	0.073
21	Jul.'99	0.074
22	Sep.'99	0.075

One such feature is the bed equilibrium profile. Table 2 contains Dean's coefficients derived upon least square fit to the measurements. They define equilibrium profiles, which may serve as predictor to the measurements treated as predictand, over the entire stretch 100–900 m. The performed CCA analysis illustrates to what extent equilibrium profiles control different portions of beach profiles. The value $P^{\otimes} = 0.555$ suggests that more than 50% of overall variability can be attributed to variations of equilibrium profiles. The line of standard deviations of prediction errors is plotted as an intermittent line in Fig. 3 and matches the patterns of previous analyses and the line of standard deviations of measurement errors. The average prediction and measurement errors over the entire profile equal $w = 0.39$ m and $\delta = 0.57$ m respectively. The quantity $\tau = 1 - (w/\delta)^2$ equals 0.53, is

almost equal to $P^{\otimes}$, and is another estimate of the percentage of explained variance. The quantities w, δ and τ for inner bars, computed over the subset (100–400 m), are equal to 0.485 m, 0.627 m and 0.40 respectively. Consequently, for the stretch 100–600 m representing bars 1, 2 and 3 we have $w = 0.45$ m, $\delta = 0.625$ m and $\tau = 0.49$. Finally, for 700–900 m $w = 0.22$ m, $\delta = 0.46$ m and $\tau = 0.78$. The CCA analyses, done separately, give very similar results. For Dean profiles at 610–900 m as the predictor and bed records 100–400 m as the predictand we obtain $P^{\otimes} = 0.45$ and $w = 0.47$ m. For the same predictor and predictand bed records 100–600 m we get $P^{\otimes} = 0.53$ and $w = 0.44$ m. We can thus see that from the analysis over the entire line 100–900 m with Dean profiles as predictor we can deduce the outcome of partial CCA computations over the profile subsets very accurately.

The above results demonstrate inner bars 1 and 2, and depend much less on equilibrium profiles ($\tau = 0.4$, $P^{\otimes} = 0.45$) than the outermost bar 4 ($\tau = 0.78$). Since changes in equilibrium profiles depict vertical profile variability we may therefore conclude that the outermost bar is dominated by vertical fluctuations, whereas for inner bars vertical movements play a less crucial role.

The comparison of all results implies that of 60% of total variability of inner bars that can be explained by variability of outer bars, some 40% can be attributed to vertical oscillations of the whole profile, expressed by changes in the Dean coefficient of the bed equilibrium line. Hence, the remaining 20% should be entailed by horizontal onshore-offshore oscillations of outer bars. Some support of this reasoning can be found in Pruszak et al. (1999), who argue that inner and outer bars are two sub-systems. They discern sub-systems upon the fact that, however gently, bar crests within both sub-systems are positively correlated, while between sub-systems the correlation is negative. In other words, we can expect that onshore movement of inner sub-systems and seaward movement of outer bars tend to occur together and vice versa. Consequently, favourable conditions should result in doubling of crest in bars 2 or 3 or their complete merger, leading to a 3 bar profile. Interestingly, such situations were encountered and are part of the data used in the CCA investigations. Since Fig. 3 shows bar crests are fairly stable profile characteristics, their positions are not accidental and therefore counter-movements of both sub-systems may account for 20% of variability of inner bars. It should be remembered though, that the above reasoning is not solid evidence but indicates directions of further research.

The results presented above suggest that 40% of variability of inner bars should be driven by phenomena not related to outer bars. They should include breakers over inner bars of mild waves that are barely affected by outer bars, longshore and cross-shore wave driven currents and interactions between shoreline and inner bars. Minor impacts could be attributed to self-organized behaviour of inner bars, such as spells of deterministic chaos, detected in movements of shoreline positions, Różyński et al. (2000). In fact Pruszak et al. (1999) found that the movements

of shoreline and inner bars were indeed positively coupled and added shoreline positions to the sub-system of inner bars. As regards mild waves and wave driven currents, we believe a separate CCA analysis of wave climate and/or wave driven currents as a predictor and bed topography in the vicinity of inner bars as such could help gain further insight into bar formation and evolution substantially.

5. Conclusions

The study demonstrated the potential and usefulness of the CCA method for studies of complex multi-bar coastal systems. By applying CCA it was found that some 60% of variability of inner bars at the study area be explained by variations of one or two outer bars, no matter what predictor we take. When Dean equilibrium profiles, depicting vertical profile variability, were adopted as the predictors, they appeared to account for 40% of variability of inner bars. Together with the previous study, it suggests that counter-movements of inner and outer bars may be held responsible for a further 20%. This however is not based on solid evidence but only on reasoning, but anyway it affords guideline for further research.

The remaining 40% of variations in inner bars should be attributed to local interactions of inner bars and mild waves, uninterrupted by outer bed forms, wave driven currents and interactions of shoreline movements and inner bars. More research is required to work out any conclusive results for those phenomena and the use of the CCA method for waves and/or currents as a predictor and bed topography as a predictand should be recommended.

Roughly 80% variability of the outermost bar can be explained by changes in the bed equilibrium profile. Such a result cannot be surprising, since this bar is always long and flat, so it can hardly move horizontally as one entity. Moreover, its depth prevents the influence of most waves, apart from storms, when the equilibrium profile undergoes the most severe changes as well.

References

Aubrey D. G. (1979), Seasonal patterns of onshore/offshore sediment movement, *Journal of Geophysical Research*, 84(C10), 6347–6354.

Barnett T. P., Preisendorfer R. (1987), Origins and levels of monthly and seasonal forecast skill for United States surface air temperatures determined by canonical correlation analysis, *Monthly Weather Review*, 115, 1825–1850.

Davis R. E. (1976), Predictability of sea surface temperatures and sea level pressure over the North Pacific Ocean, *Journal of Physical Oceanography* 6, 249–266.

Davis R. E. (1978), Predictability of sea level pressure over the North Pacific Ocean, *Journal of Physical Oceanography* 8, 233–246.

De Vriend H. J. (1991), Mathematical modeling and large-scale coastal behavior. Part 1: Physical processes, *Journal of Hydraulic Research*, 29(6), 727–740.

Glahn H. R. (1968), Canonical correlation analysis and its relationship to discriminant analysis and multiple regression, *Journal of Atmospheric Sciences* 25, 23–31.

Graham N. E., Michaelsen J., Barnett T. P. (1987a), An investigation of the ENSO cycle with statistical models. 1. Predictor field characteristics, *Journal of Geophysical Research* 92, 14251.

Graham N. E., Michaelsen J., Barnett T. P. (1987b), An investigation of the ENSO cycle with statistical models. 2. Model results, *Journal of Geophysical Research* 92, 14271.

Graham N. E. (1990), Canonical correlation analysis, *WMO review of climate diagnostic models*.

Hasselmann K. (1988,) PIPs and POPs: The reduction of complex dynamical systems using principal interaction and oscillation patterns, *Journal of Geophysical Research*, 93(D9), 11,015–11,021.

Hotelling H. (1935), The most predictable criterion, *J. Ed. Psych.*, 26, 139–142.

Larson M. and Kraus N. C. (1995), Prediction of cross-shore sediment transport at different spatial and temporal scales, *Marine Geology*, 126, 111–127.

Larson M., Hanson H., Kraus N. C., Newe J. (1999), Short- and long-term responses of beach fills determined by EOF analysis, *Journal of Waterways, Port, Coastal, and Ocean Engineering*, 125(6), 285–293.

Larson M., Capobianco M., Hanson H. (2000a), Relationship between beach profiles and waves at Duck, North Carolina, determined by canonical correlation analysis, *Marine Geology*, (in press).

Larson M., Capobianco M., Jansen H., Różyński G., Southgate H., Stive M., Wijnberg K. (2000b), Analysis and modeling of field data on coastal morphological evolution over yearly and decadal time scales. Part 1: Background and linear techniques, *Journal of Coastal Research*, (submitted).

Pruszak Z., Różyński G., Zeidler R. B. (1997), Statistical properties of multiple bars, *Coastal Engineering*, 31, 263–280.

Pruszak Z., Różyński G., Szmytkiewicz M., Skaja M. (1999), Quasi-seasonal morphological shore evolution response to variable wave climate, *Proc. Coastal Sediments '99 Conference*, ASCE 1081–1093.

Różyński G., Pruszak Z., Okrój T., Zeidler R. B. (1999), Depth of closure and seabed variability patterns, *Proc. ICCE'98*, ASCE 2926–2939.

Różyński G., Jansen H. (2000), Modeling nearshore bed topography with principal oscillation patterns, *Journal of Waterways, Port, Coastal and Ocean Engineering* (in press).

Różyński G., Larson M., Pruszak Z. (2000), Forced and self-organized shoreline response for a beach in the southern Baltic Sea determined through singular spectrum analysis (SSA), *Coastal Engineering* (in press).

Southgate H. N., Wijnberg K. M., Larson M., Capobianco M., Jansen H. (2000), Analysis of field data of coastal morphological evolution over yearly and decadal time scales. Part 2: Non-linear techniques, *Journal of Coastal Research* (submitted).

Vautard R., Yiou P., Ghil M. (1992), Singular spectrum analysis: A toolkit for short, noisy, chaotic signals, *Physica* D, 58: 95–126.

Wijnberg K. M., Terwindt J. H. J. (1995), Extracting decadal morphological behaviour from high-resolution, long-term bathymetric surveys along the Holland coast using eigenfunction analysis, *Marine Geology*, 126, 301–330.

Winant C. D., Inman D. L., Nordstrom C. E. (1975), Description of seasonal beach changes using empirical eigenfunctions, *Journal of Geophysical Research*, 80(15), 1979–1986.